JOURNAL OF GUIDANCE, CONTROL, AND DYNAMICS
Vol. 32, No. 1, January–February 2009

Coordinated Standoff Tracking of Moving Targets: Control Laws and Information Architectures

Tyler H. Summers* and Maruthi R. Akella†
University of Texas at Austin, Austin, Texas 78712
and
Mark J. Mears‡
U.S. Air Force Research Laboratory,
Wright–Patterson Air Force Base, Ohio 45433

DOI: 10.2514/1.37212

In this paper, we present work on the control of autonomous vehicle formations in the context of the coordinated standoff tracking problem. The objective is to use a team of unmanned aircraft to fly a circular orbit around a moving target with prescribed intervehicle angular spacing using only local information. We use the recently introduced Lyapunov guidance vector field approach to achieve the desired circular trajectory. The contributions of this paper involve both single-vehicle path planning and multiple-vehicle coordination. For single-vehicle path planning, we complete a proof of heading convergence using feedback, which has thus far not been fully addressed in the literature. We also offer a novel approach for heading convergence that does not require continuous feedback in the ideal case (no wind, stationary target), taking advantage of an analytical solution for the guidance field. Further, we use a variable airspeed controller to maintain the circular trajectory despite unknown wind and unknown constant velocity target motion. Adaptive estimates of the unknown wind and target motion are introduced to ensure stability of the circular trajectory. A novel feature of our results is rigorous satisfaction of vehicle-specific kinematic constraints on heading rates and airspeed variations. For multiple-vehicle coordination, we again use a variable airspeed controller to achieve the prescribed angular spacing. We make a connection with some recent work that addresses information architecture in vehicle formations using rigid graph theory. Specifically, we discuss two types of information architectures, symmetric and asymmetric, and implement decentralized control laws that are based on these architectures. The information architectures are scalable in that the number of required communication/sensing links increases linearly with the number of vehicles. The control laws are decentralized in that they use only local information.

I. Introduction

FORMATIONS of autonomous vehicles are increasingly being deployed to accomplish a variety of tasks in a coordinated way. Teams of small, relatively inexpensive unmanned aerial vehicles (UAVs), each equipped with sensing, communication, computation, and control capabilities, can provide distributed sensing and can be designed to be robust to the failure of a single vehicle. The overarching requirement for large formations is that implementation of the design be decentralized and scalable to any number of vehicles. It is infeasible to have a single centralized agent that handles tasks for the whole formation. Control, communication, sensing, and computation tasks must be handled on a decentralized basis, giving rise to the significant technical challenges of formation control.

There has been a proliferation of research efforts to study many aspects of cooperatively controlling formations of autonomous vehicles [1–12]. This work tends to fall into the broad categories of vehicle path planning, optimal sensing geometry, decentralized control law design, and information architectures. It is increasingly apparent that these various aspects of the cooperative control problem need to be unified into a general framework. This is a formidable task, not only because there are many important aspects of the problem, but also because these aspects are interrelated in nontrivial ways. This paper is concerned with making a modest step toward such a general framework by bringing together two key aspects: decentralized control law design, which accounts for kinematic constraints, and scalable information architectures. We will illustrate this convergence via the *coordinated standoff tracking problem*.

A primary use of UAVs is the surveillance and tracking of moving targets. Teams of UAVs could be employed to engage and assess unknown or adversarial targets to provide reconnaissance or to provide surveillance of the surrounding area for potential threats to a friendly convoy. In the coordinated standoff tracking problem, a typical objective is to use a team of UAVs to fly a circular orbit around a moving target with prescribed intervehicle angular spacing using only local information. An optimal configuration for gathering information about a given target is one that places vehicles at equal angular spacing around a perimeter [13]. Recently, Frew and Lawrence introduced a Lyapunov guidance vector field approach to maintaining the prescribed standoff radius [14]. However, their study neglected an important timescale separation issue involving heading and standoff radius convergence. Further, their analysis of two vehicles that vary their respective airspeeds to accomplish a prescribed angular spacing while executing a circular orbit around the target did not provide a formal proof of convergence. Kingston and Beard also adopted a Lyapunov guidance vector field approach to the problem and used heading control exclusively to obtain the desired circular orbit and spacing [15]. Their study circumvented the timescale separation issue by using a sliding mode controller to guarantee heading convergence in finite time. It also used a

Received 18 February 2008; revision received 27 August 2008; accepted for publication 27 August 2008.

*Ph.D. Student, Department of Aerospace Engineering and Engineering Mechanics, 1501 Barton Springs Road; thsummers@mail.utexas.edu. Student Member AIAA.

†Associate Professor, Department of Aerospace Engineering and Engineering Mechanics; makella@mail.utexas.edu. Associate Fellow AIAA.

‡Control Systems Engineer, Air Vehicles Directorate; mark.mears@wpafb.af.mil.

symmetric information structure that scales to n vehicles and gives some local stability results, although their Monte Carlo analysis also suggested global stability.

In this paper, we further develop the Lyapunov guidance vector field approach to guide vehicles to the desired circular orbit. We provide a proof of convergence that addresses the timescale separation issue and propose a novel approach for heading convergence that does not require feedback in the ideal case (no wind, stationary target) and that takes advantage of an analytical solution to the guidance field. Further, we use a variable airspeed controller and adaptive estimates of unknown wind and target motion to maintain the circular orbit. Three novel features of our results are 1) the rigorous satisfaction of vehicle-specific kinematic constraints on heading rates and airspeed variations, 2) the use of a variable airspeed controller to achieve the prescribed angular spacing for multiple-vehicle coordination, and 3) the establishment of new connections with recent work in rigid graph theory. Specifically, we model the information architecture with a graph $G(V, E)$, where V is a set of vertices representing vehicles and E is a set of edges representing information flow amongst the vehicles. We show that a graph property called *rigidity* is desired to achieve the objective of the coordinated standoff tracking problem. We describe two types of information architectures, symmetric and asymmetric, and use them to inform our design of the decentralized control laws. These information architectures are scalable to any number of vehicles in that the number of required communication/sensing links increases linearly with the number of vehicles. The implementation of the control laws is decentralized in that they use only local information.

The paper is organized as follows. In Sec. II, we present the dynamic model and the Lyapunov guidance field approach. In the no-wind, stationary target case, we show that the guidance field admits a closed-form analytical solution and that this can be used in a path planning approach for a single vehicle. We analyze two approaches for heading convergence, including a novel approach that guarantees exact heading convergence in finite time, and demonstrate that trajectory is entirely determined from the initial condition. In Sec. III, we apply these results to the moving target case (of unknown constant velocity) with wind. Adaptive estimates are used to account for wind and nonaccelerating target motion to achieve the desired circular orbit and angular spacing. To the best of the authors' knowledge, this is the first time such a result has been presented. In Sec. IV, we review some recent work that relates graph theoretic concepts to formation control to associate meaningful information architectures to our decentralized control laws. In Sec. V, we present a variable airspeed control law that achieves the desired angular spacing using two different information architectures. We show global convergence for any number of vehicles for both architectures. In Sec. VI, we show the results of some numerical simulations and, in Sec. VII, we offer some concluding remarks and potential future research directions.

II. Model

This section presents the dynamic model and the Lyapunov guidance vector field approach to guiding a single vehicle to the desired circular orbit. We begin with the no-wind, stationary target case and generalize the results to account for unknown wind and target motion in the following section.

A. Lyapunov Guidance Vector Field Construction

We use the following unicycle model with kinematic constraints to describe the dynamics of a fixed-wing UAV:

$$\dot{x} = u_1 \cos\psi, \qquad \dot{y} = u_1 \sin\psi, \qquad \dot{\psi} = u_2 \tag{1}$$

where $[x, y]^T \in R^2$ is the inertial position of the aircraft, ψ is the heading, u_1 is the commanded airspeed, and u_2 is the commanded heading. This model, as with any model, represents a simplification of the physics of a real UAV. It is assumed that the UAV is capable of altitude stabilization, and so the analysis is restricted to a flat-Earth plane and second-order dynamics typically associated with the control inputs are neglected. However, the unicycle model has been used extensively in the literature [14,16,17] and is a reasonable starting point for describing UAV motion. We have strived to enforce kinematic constraints that would be an essential feature of any practical implementation. We assume that there are constraints on the minimum and maximum airspeed according to

$$0 < v_{\min} \le u_1 \le v_{\max} \tag{2}$$

and a constraint on the maximum heading rate magnitude according to

$$|u_2| \le \omega_{\max} \tag{3}$$

The maximum heading rate constraint is equivalent to a minimum turning radius constraint, where $r_{\min} = 4u_1/\omega_{\max}$.

The heading and airspeed commands are generated from a Lyapunov vector field that guides the UAV to a circular orbit around the target, which is assumed to be stationary and centered at the origin. Consider the Lyapunov function

$$V(r) = \tfrac{1}{2}\left(r^2 + r_d^2\right)^2 \tag{4}$$

where $r = \sqrt{x^2 + y^2}$ is the relative distance to the target and r_d is the desired standoff radius of the circular orbit. To achieve the circular orbit, we choose the desired inertial velocity according to the vector field

$$f(x, y) = \begin{bmatrix} \dot{x} \\ \dot{y} \end{bmatrix} = -\frac{u_0}{r\left(r^2 + r_d^2\right)} \begin{bmatrix} x\left(r^2 - r_d^2\right) + y(2rr_d) \\ y\left(r^2 - r_d^2\right) - x(2rr_d) \end{bmatrix} \tag{5}$$

where u_0 is the constant nominal vehicle airspeed. This field may be expressed in polar coordinates as

$$g(r, \theta) = \begin{bmatrix} \dot{r} \\ r\dot{\theta} \end{bmatrix} = \frac{u_0}{r^2 + r_d^2} \begin{bmatrix} -\left(r^2 - r_d^2\right) \\ 2rr_d \end{bmatrix} \tag{6}$$

Observe qualitatively that when $r > r_d$, r decreases toward the standoff radius; when $r < r_d$, r increases toward the standoff radius; and when $r = r_d$, r is constant and the vehicle moves around the standoff circle with a constant angular velocity of $\dot{\theta} = u_0/r_d$, which is the desired behavior. Evaluating the derivative of Eq. (4) along these trajectories, then

$$\dot{V} = -\frac{4u_0 r\left(r^2 - r_d^2\right)^2}{r^2 + r_d^2} \le 0 \tag{7}$$

and LaSalle's invariance principle may be invoked to conclude that the trajectories converge asymptotically to the desired standoff radius [14].

In fact, the vector field admits a closed-form analytical solution. Observe that the dynamics in Eq. (6) are independent of θ, and we can obtain

$$\frac{\mathrm{d}r}{\mathrm{d}\theta} = -\frac{r^2 - r_d^2}{2rr_d} \tag{8}$$

which has the solution

$$r(\theta) = \frac{1 + k_r e^{-\theta}}{1 - k_r e^{-\theta}} r_d, \qquad k_r = \frac{r_0 - r_d}{r_0 + r_d} \tag{9}$$

where $r_0 = r(0)$ is the initial separation distance from the target. This solution may be substituted into the $\dot{\theta}$ equation in Eq. (6), which may be integrated to give the following solution as a function of time:

$$\theta - \theta_0 = \frac{u_0}{r_d} t + 2k_r \left[\frac{e^{-\theta}}{1 - k_r e^{-\theta}} - \frac{e^{-\theta_0}}{1 - k_r e^{-\theta_0}}\right] \tag{10}$$

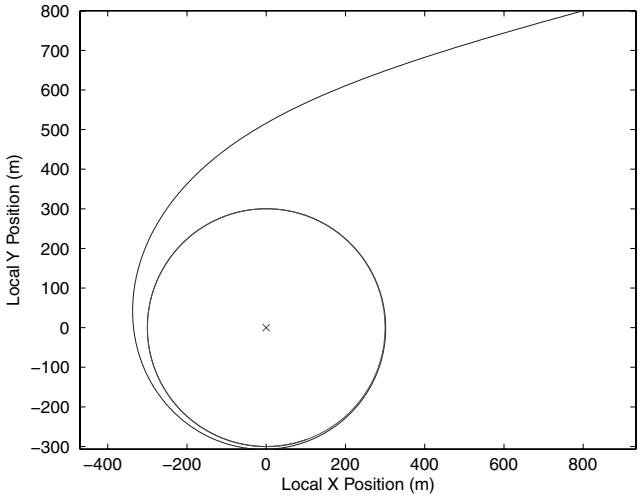

Fig. 1 Guidance field trajectory.

where θ_0 is the initial polar coordinate "clock angle." An example trajectory is shown in Fig. 1 with $u_0 = 20$ m/s, $r_d = 300$ m, $x_0 = 800$ m, and $y_0 = 800$ m.

The solutions given by Eqs. (9) and (10) constitute the complete analytical solution to the guidance vector field; hence, the exact trajectories on the field are known. The desired heading along the vector field, denoted by ψ_d, is determined from Eq. (5) via

$$\psi_d = \arctan\left(\frac{\dot{y}}{\dot{x}}\right) = \arctan\left(\frac{y\left(r^2 - r_d^2\right) - x(2rr_d)}{x\left(r^2 - r_d^2\right) + y(2rr_d)}\right) \tag{11}$$

Differentiating, we obtain the desired heading rate along the guidance field

$$\dot{\psi}_d = \frac{4u_0 r_d^3}{\left(r^2 + r_d^2\right)^2} \tag{12}$$

To satisfy the heading rate constraint, we require $|\dot{\psi}_d| < \omega_{\max}$, which can be written in terms of u_0 and r_d as $4u_0/r_d < \omega_{\max}$.

We have shown that a vehicle with a heading commanded according to Eq. (11) will converge to the desired circular orbit, provided that the initial heading is aligned with the guidance field. However, in general, the initial vehicle heading will not be aligned with the guidance field and we need an approach to converge to the desired heading.

B. Heading Convergence

A heading feedback approach to obtaining exponential heading convergence is used by Frew and Lawrence; however, a complete proof that accounts for the timescale separation between the heading convergence and standoff radius convergence is absent [14]. Other studies use a sliding mode controller to guarantee heading convergence in a finite time [15,18], which is inherently discontinuous and known to produce actuator chatter. This problem is typically circumvented in practice by an approximation via a saturation function, but this has the effect of diluting the theoretical convergence properties.

In this subsection, we present a proof of heading convergence using the feedback approach that explicitly addresses the timescale separation issue. We also identify two theoretical and practical problems with this approach. First, the proof of convergence is restricted to a certain set of initial headings and, second, the kinematic constraints are not always satisfied.

As an alternative, we propose a novel, yet simple, approach to heading convergence, which involves an initial minimum radius loiter circle. The vehicle converges exactly to the desired heading in finite time for any initial heading and does not violate the kinematic constraints. Further, the time and location of convergence are analytically available, and this allows the entire trajectory to be exactly known for any arbitrary initial heading.

1. *Heading Feedback*

Before proceeding with the heading error analysis, we introduce some additional notation for the guidance trajectories. Because $x = r\cos\theta$ and $y = r\sin\theta$, we define the angle ϕ via

$$\cos\phi = \frac{r^2 - r_d^2}{r^2 + r_d^2}, \qquad \sin\phi = \frac{2rr_d}{r^2 + r_d^2} \tag{13}$$

and we can write the vehicle dynamics (5) as

$$\begin{aligned}\dot{x} &= -\frac{u_0}{r^2 + r_d^2}\left[\left(r^2 - r_d^2\right)\frac{x}{r} + (2rr_d)\frac{y}{r}\right] \\ &= -u_0[\cos\theta\cos\phi + \sin\theta\sin\phi] = -u_0\cos(\theta - \phi)\end{aligned} \tag{14}$$

and, similarly,

$$\begin{aligned}\dot{y} &= -\frac{u_0}{r^2 + r_d^2}\left[\left(r^2 - r_d^2\right)\frac{y}{r} - (2rr_d)\frac{x}{r}\right] \\ &= -u_0[\sin\theta\cos\phi - \cos\theta\sin\phi] = -u_0\sin(\theta - \phi)\end{aligned} \tag{15}$$

Accordingly, from Eq. (13) we obtain the following angle relationship:

$$\psi_d = \theta - \phi + \pi \tag{16}$$

Now, suppose the vehicle has some initial heading error ψ_e defined by

$$\psi_e = \psi - \psi_d \tag{17}$$

where ψ is the actual heading and ψ_d is the desired heading along the guidance solution. If the heading rate input u_2 is given by

$$u_2 = -k\psi_e + \dot{\psi}_d \tag{18}$$

for some feedback gain of $k > 0$, then we obtain exponential convergence of the feedback error as $\psi_e(t) = \psi_{e0}e^{-kt}$, wherein $\psi_{e0} = \psi_e(0)$. Note that the parameter k explicitly governs the heading error convergence rate and that k must be chosen so that the turn rate constraint given by Eq. (3) is not violated. This requires striking a proper balance between the feedback and feedforward terms in Eq. (18).

From Eqs. (1) and (17), the vehicle dynamics may be expressed as

$$\begin{bmatrix}\dot{x} \\ \dot{y}\end{bmatrix} = \begin{bmatrix}\cos(\psi_e) & -\sin(\psi_e) \\ \sin(\psi_e) & \cos(\psi_e)\end{bmatrix}\begin{bmatrix}u_1\cos(\psi_d) \\ u_1\sin(\psi_d)\end{bmatrix} \tag{19}$$

Note that the matrix involving the heading error has the structure of a rotation matrix. Further, as the heading error $\psi_e(t)$ converges to zero, this matrix exponentially becomes the identity matrix, and the ideal dynamics along the guidance field are recovered. From Eq. (19), we obtain the desired heading rate when there is a heading error:

$$\begin{aligned}\dot{\psi}_d = \frac{4u_0 r_d^3}{(r^2 + r_d^2)^2} - \frac{2u_0}{r}\sin\left(\frac{\psi_e}{2}\right)\Bigg[\cos\left(\phi - \frac{\psi_e}{2}\right) \\ - \sin(\phi)\sin\left(\phi - \frac{\psi_e}{2}\right)\Bigg]\end{aligned} \tag{20}$$

The desired heading rate here consists of the ideal heading rate along the guidance field given in Eq. (12) and a term involving $\sin(\psi_e/2)$ that goes to zero as ψ_e goes to zero. This additional term involves r in the denominator and may produce large heading rate commands that would violate the heading rate constraint when r becomes small.

The results for boundedness and convergence with the heading feedback approach depend on the quadrant of the initial heading error, illustrated in Fig. 2 in which the curve represents the analytical guidance trajectory with $u_0 = 20$ m/s, $r_d = 300$ m, $x_0 = 600$ m,

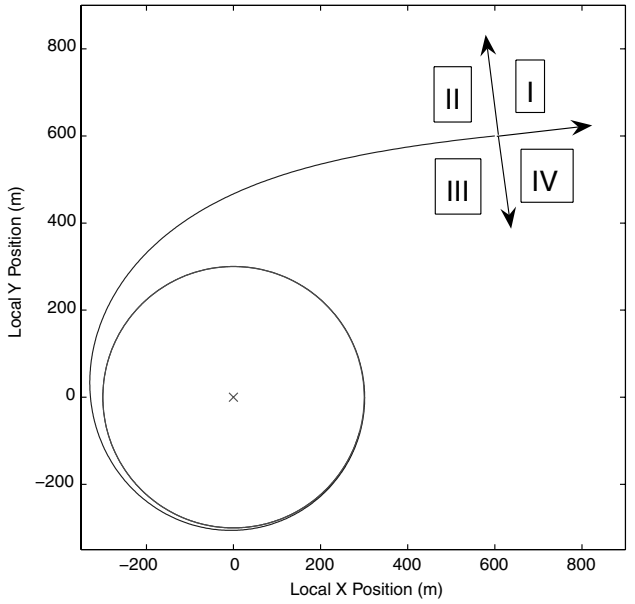

Fig. 2 Heading error quadrants.

and $y_0 = 600$ m. The desired heading is tangent to this trajectory; in general, the actual initial heading will not be aligned with the guidance field, but instead pointed in the direction of one of the quadrants shown. The result is provided by the following theorem.

Theorem 1. Suppose the vehicle dynamics are given by Eq. (1) and subject to kinematic constraints (2) and (3). Suppose the airspeed input is set to a constant u_0 and the heading rate input is given by (18) and (20). Then. when the initial heading error satisfies $-\pi/2 \leq \psi_{e0} \leq \pi/2$ (i.e., the heading error is in quadrant II or III, as shown in Fig. 2), the vehicle asymptotically converges to the standoff radius and circles the target with a constant angular velocity, that is, $\lim_{t\to\infty} r(t) = r_d$ and $\lim_{t\to\infty} \dot{\theta}(t) = u_0/r_d$.

Proof. The vehicle dynamics may be expressed in polar coordinates as

$$\begin{bmatrix} \dot{r} \\ r\dot{\theta} \end{bmatrix} = \frac{u_0}{r^2 + r_d^2} \begin{bmatrix} \cos(\psi_e) & -\sin(\psi_e) \\ \sin(\psi_e) & \cos(\psi_e) \end{bmatrix} \begin{bmatrix} -\left(r^2 - r_d^2\right) \\ 2rr_d \end{bmatrix} \tag{21}$$

We can express the r dynamics more compactly as

$$\dot{r} = -u_0 \cos(\phi - \psi_e) \tag{22}$$

Let us first establish an upper bound for r. Note from Eq. (13) that $\phi \in [0, \pi)$ (because $r \geq 0$) and $\phi \to 0$ as $r \to \infty$, $\phi = \pi/2$ when $r = r_d$, and $\phi \to \pi$ as $r \to 0$.

For the first case, suppose that the initial heading error is $-\pi/2 \leq \psi_{e0} < 0$ (i.e., the heading error is in quadrant II). Then we obtain the following upper bound on r (assuming $r_0 > r_d$):

$$r(t) \leq r_0 + u_0 t^* \triangleq r_{\sup} \tag{23}$$

where t^* is the time at which r achieves its maximum value, which may be bounded as

$$t^* \leq \frac{1}{k} \ell_n \left(\frac{-\psi_{e0}}{\frac{\pi}{2} - \phi(0)} \right) \tag{24}$$

From Eq. (22) we have $r(t) \geq r_d$ for all $t \geq 0$.

For the second case, suppose that $0 \leq \psi_{e0} \leq \pi/2$ (i.e., the initial heading error is in quadrant III). From Eq. (22) we obtain $r(t) \leq r_0 \leq r_{\sup}\ \forall t$. For this case, it is possible for $r(t)$ to become smaller than the prescribed standoff radius r_d. The actual size of this standoff distance violation effectively depends on the initial distance to the target r_0 and the feedback gain parameter k.

Now consider the Lyapunov function candidate:

$$V = \tfrac{1}{2}\left(r^2 - r_d^2\right)^2 + (\lambda/2)\psi_e^2 \tag{25}$$

for some $\lambda > 0$. Evaluating $\dot{V}$ along the trajectories given by Eqs. (21) and (22), then

$$\dot{V} = \frac{-2u_0 r\left(r^2 - r_d^2\right)^2}{r^2 + r_d^2} + 4u_0 r\left(r^2 - r_d^2\right) \sin\left(\frac{\psi_e}{2}\right) \sin\left(\frac{\psi_e}{2} - \phi\right) - \lambda k \psi_e^2 \tag{26}$$

Now, provided that $-\pi/2 \leq \psi_{e0} \leq \pi/2$, we can bound $\dot{V}$ as

$$\dot{V} \leq \frac{-u_0 r\left(r^2 - r_d^2\right)^2}{r^2 + r_d^2} + \left[u_0 r_{\sup}\left(r_{\sup}^2 + r_d^2\right) - \lambda k\right]\psi_e^2 \tag{27}$$

and choosing λ according to

$$\lambda > (1/k) u_0 r_{\sup}\left(r_{\sup}^2 + r_d^2\right) \tag{28}$$

we then obtain

$$\dot{V} \leq \frac{-u_0 r\left(r^2 - r_d^2\right)^2}{r^2 + r_d^2} - \alpha \psi_e^2 \leq 0 \tag{29}$$

where $\alpha > 0$. Thus, $\lim_{t\to\infty} r(t) = r_d$, and $\lim_{t\to\infty} \dot{\theta}(t) = u_0/r_d$ follows from Eq. (21). When $|\psi_{e0}| > \pi/2$ (i.e., the heading error is in quadrant I or IV), we cannot bound $\dot{V}$ as earlier. Consequently, the proof does not encompass this range of initial headings.

Our proof of convergence addresses the timescale separation issue between the heading convergence and the standoff radius convergence. The theoretical problem with this approach is that the proof is restricted to the initial headings in quadrants II and III. It is not necessarily impossible to prove convergence for the remaining quadrants, though it would likely require a nontrivial modification to what we have shown. The practical problem with this approach is that, for the initial headings in quadrant III, where $r(t)$ could possibly become smaller than the prescribed standoff distance r_d, it is not straightforward to choose the heading feedback gain k in such a way to satisfy the heading rate constraint. The lower bound of r for the initial headings in quadrant III is a function of k, and there is potential to violate the heading rate constraint. A particular case is shown in Fig. 3 with $u_0 = 20$ m/s, $r_d = 300$ m, $x_0 = 325$ m, $y_0 = 0$ m, $\psi_0 = \pi$, and $k = 0.001$. Although the trajectory will eventually converge to the standoff radius via Theorem 1, it gets close to the

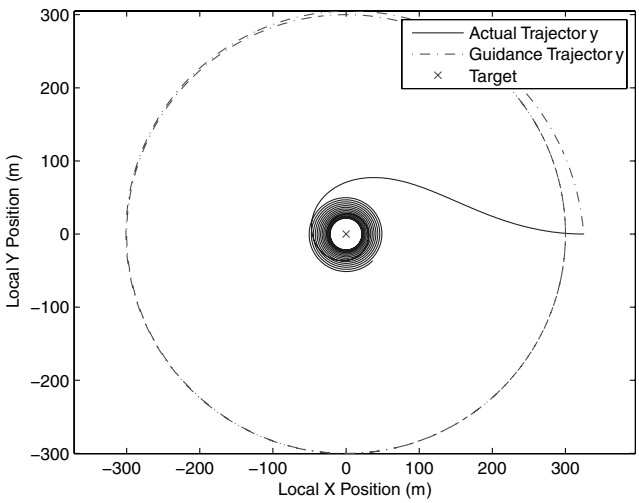

Fig. 3 Trajectory using heading feedback with initial heading in quadrant III and small feedback gain.

target in the process and potentially violates the turn rate constraint due to the tighter loops the vehicle must execute around the target.

2. Initial Loiter Circle

The availability of an analytical solution for the guidance vector field motivates a novel approach for aligning the heading with the field. In particular, we show in this subsection that the desired heading can be exactly achieved without the use of a continuous heading feedback. The approach is to fly an initial loiter circle of minimum radius $r_{\min}$ that is consistent with the heading rate constraint (3). Whenever the desired heading is exactly achieved, the vehicles can switch onto the guidance field solution, which is analytically known from Eqs. (9) and (10). The time and location of convergence are analytically available. The result is given by the following theorem.

Theorem 2. Any minimum radius loiter circle that does not contain the target, that is, $r_0 > r_d + r_{\min}$, will necessarily obtain the desired heading defined by the guidance vector field (11) within a finite time.

Proof. Consider a minimum radius loiter circle on which a vehicle is initially traveling. This trajectory continuously takes on all values in $[0, 2\pi]$ from the initial time to the time it takes to complete the loiter circle. Note that the desired heading on the loiter circle is the same at the initial time and at the time at which a loiter circle has been completed (because this is the same point in space). Assuming that the loiter circle does not contain the target, we can show that the desired heading along the loiter circle takes on only a subset of values in $[0, 2\pi]$. Then, along the lines of the intermediate value theorem, the headings will match at some point between the initial time and the time at which a loiter circle has been completed. We make the argument for the open right half-plane. By the radial symmetry of the guidance vector field, the argument will hold for any rotated open half-plane. Thus, the result holds for any loiter circle that does not contain the target.

Let us show that in the open right half-plane the guidance vector field (5) never points down, that is, when the $\dot{x}$ component is zero, the $\dot{y}$ component is positive. Ignoring the scalar parts because they do not contribute to direction, when the $\dot{x}$ component is zero, the $\dot{y}$ component is given by

$$\dot{y} = 2r_d(x + (y^2/x))\sqrt{x^2 + y^2} \tag{30}$$

Because in the open right half-plane $x > 0$, then $\dot{y} > 0$. By radial symmetry of the vector field, the same argument is valid for any rotated open half-plane; hence, the desired heading can be attained by any trajectory in this plane that acquires all headings. □

Thus, it suffices to simply execute an initial loiter circle of minimum radius in accordance with the initial heading, and the desired heading will be exactly attained in finite time at some point on the circle. In fact, in the stationary target with no-wind case, we can determine the point of heading convergence as follows. Consider an initial loiter circle defined by

$$(x - x_l)^2 + (y - y_l)^2 = r_{\min}^2 \tag{31}$$

where (x_l, y_l) defines the center of the initial loiter circle and $r_{\min}$ denotes the minimum turn radius according the heading rate constraint (3). We can rewrite this equation in polar coordinates as

$$r^2 + r_{\min}^2 - r_l^2 - 2rr_{\min}\cos(\theta - \alpha) = 0 \tag{32}$$

where $r_l = \sqrt{x_l^2 + y_l^2}$ and α is the clock angle relative to horizontal reference direction on the initial loiter circle defined by

$$x - x_l = r_{\min}\cos\alpha, \qquad y - y_l = r_{\min}\sin\alpha \tag{33}$$

The angle α is related to the heading as

$$\psi = \alpha + (\pi/2) \tag{34}$$

We are seeking the point where $\psi_d = \psi$, and from Eqs. (16) and (34) we can obtain the following relationship:

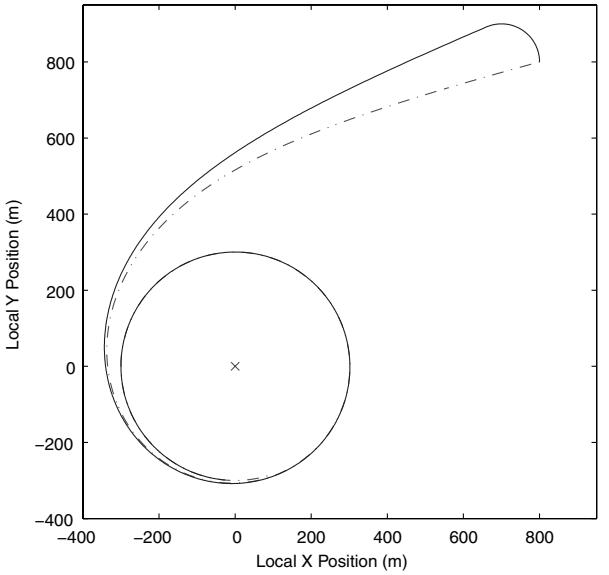

Fig. 4 Trajectory using initial left-turn loiter circle to converge exactly to the desired heading.

$$\theta - \alpha = \phi - (\pi/2) \tag{35}$$

which implies

$$\cos(\theta - \alpha) = \sin\phi \tag{36}$$

From the definition of ϕ, Eq. (32) can be written as

$$r^4 + \left(r_{\min}^2 - r_l^2 + r_d^2 + 4r_d r_{\min}\right)r^2 + r_d^2\left(r_{\min}^2 - r_l^2\right) = 0 \tag{37}$$

and the real, positive solution to this equation corresponds to the point on Eq. (31) at which the desired heading will be obtained. An example trajectory using this approach is shown in Fig. 4.

Further, we can implement logic on the turn direction of the initial loiter circle to minimize the time to heading convergence and also the penetration depth of the standoff radius, which may be desired for adversarial targets for which stealth is needed. Referring back to the heading error quadrants defined in Fig. 2, it is reasonable to choose a left-turn loiter when the heading error is in quadrants I and II, and a right-turn loiter when the heading error is in quadrants III and IV. As examples, Fig. 4 shows a case in which a left-turn loiter is executed with $u_0 = 20$ m/s, $r_d = 300$ m, $x_0 = 800$ m, and $y_0 = 800$ m and $\psi_0 = \pi/2$, and Fig. 5 shows a case where a right-turn loiter is executed with $u_0 = 20$ m/s, $r_d = 300$ m, $x_0 = 800$ m, and $y_0 = 800$ m and $\psi_0 = -\pi/2$. Moreover, when the initial radius satisfies $r_0 < r_d + 2r_{\min}$ and it is desirable to avoid penetrating the standoff radius, a left-turn loiter may be executed with quadrant IV headings. This case is shown in Fig. 6 with $u_0 = 20$ m/s, $r_d = 300$ m, $x_0 = 230$ m, and $y_0 = 230$ m and $\psi_0 = -3\pi/4$.

There are several advantages to using this approach instead of the heading feedback. First, the convergence to the guidance field heading is exact, not asymptotic. As a consequence, the entire trajectory, including the analytical guidance solution, is exactly known at the initial time for arbitrary initial heading errors. Therefore, there is no need to continuously measure the heading for feedback. Measurements of deviations from this trajectory may be used to estimate unknown wind and target motion, which we show in the following section. Finally, the heading rate constraint (3) is always satisfied.

III. Moving Target Tracking with Wind

In this section we extend the Lyapunov guidance vector field approach to account for unknown wind and target motion. Specifically, we use variable airspeed control and adaptive estimates of wind and target motion to maintain stability of the circular orbit

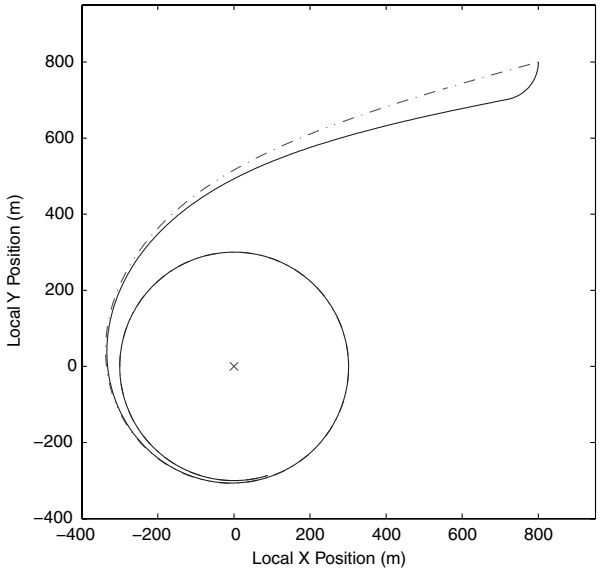

Fig. 5 Trajectory using initial right-turn loiter circle to converge exactly to the desired heading.

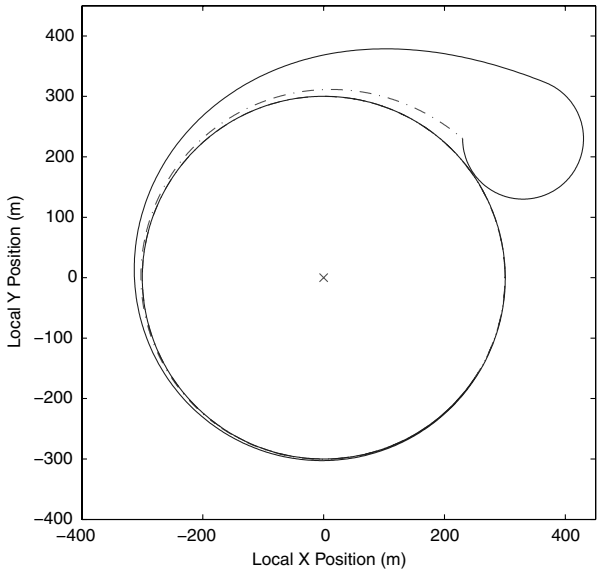

Fig. 6 Trajectory using initial left-turn loiter circle with quadrant IV heading to avoid penetrating the standoff radius.

pattern. We restrict consideration to targets moving with constant velocity, though the same principles could, in theory, be applied to a more general target motion. We also discuss theoretical and practical limitations on what can be achieved given the kinematic constraints on the controllers.

A. Variable Airspeed Controller with Adaptive Wind/Target Motion Estimates

Consider the vehicle dynamics given by Eq. (1) expressed relative to a moving target and incorporating a wind term:

$$\dot{x} = u_1 \cos\psi + W_x - V_{xT}, \qquad \dot{y} = u_1 \sin\psi + W_y - V_{yT}$$
$$\dot{\psi} = u_2 \tag{38}$$

where $[W_x, W_y]^T$ are components of the constant wind velocity and $[V_{xT}, V_{yT}]^T$ are components of the constant inertial target velocity. The wind and target velocity both affect the dynamics additively, and this allows us to combine the two effects into one variable:

$$T_x = V_{xT} - W_{x,} \qquad T_y = V_{yT} - W_y \tag{39}$$

We treat T_x and T_y as *unknown* constants and assume the a priori availability of an upper bound, T^*, satisfying

$$\max(T_x, T_y) \le T^* \tag{40}$$

which encompasses worst-case combined effect of wind and target velocities.

Consider the following controller construction:

$$u_1 \cos\psi = -u_0 \cos(\theta - \phi) + \hat{T}_x - \nu_s \sin\theta$$
$$u_1 \sin\psi = -u_0 \sin(\theta - \phi) + \hat{T}_y + \nu_s \cos\theta \tag{41}$$

where $\hat{T}_x$ and $\hat{T}_y$ are adaptive estimates for the unknown wind and target motion, ν_s is a yet-to-be-specified signal, and all other variables have the same meaning as before. This construction defines a heading given by

$$\tan\psi = \frac{-u_0 \sin(\theta - \phi) + \hat{T}_y + \nu_s \cos\theta}{-u_0 \cos(\theta - \phi) + \hat{T}_x - \nu_s \sin\theta} \tag{42}$$

and an airspeed input given by

$$u_1^2 = [-u_0 \cos(\theta - \phi) + \hat{T}_x - \nu_s \sin\theta]^2 + [-u_0 \sin(\theta - \phi) + \hat{T}_y + \nu_s \cos\theta]^2 \tag{43}$$

The heading given by Eq. (42) may be differentiated to obtain the heading rate input.

Using Eq. (41) with Eq. (38), we obtain

$$\dot{r} = -u_0 \frac{r^2 - r_d^2}{r^2 + r_d^2} + \tilde{T}_x \cos\theta + \tilde{T}_y \sin\theta$$
$$r\dot{\theta} = -u_0 \frac{2 r r_d}{r^2 + r_d^2} - \tilde{T}_x \sin\theta + \tilde{T}_y \cos\theta + \nu_s \tag{44}$$

where $\tilde{T}_x = \hat{T}_x - T_x$ and $\tilde{T}_y = \hat{T}_y - T_y$ are the adaptive estimation errors. We now use the same Lyapunov guidance field as before to define the perfect case *relative* motion:

$$\dot{r_p} = -u_0 \frac{r_p^2 - r_d^2}{r_p^2 + r_d^2}, \qquad r_p \dot{\theta}_p = -u_0 \frac{2 r_p r_d}{r_p^2 + r_d^2} \tag{45}$$

We define the error signals as

$$e_r = r - r_p, \qquad e_\theta = \theta - \theta_p \tag{46}$$

and the corresponding error dynamics are then given by

$$\dot{e}_r = -u_0 \frac{2 r_d^2 \left(r^2 - r_p^2\right) e_r}{\left(r^2 + r_d^2\right)\left(r^2 + r_p^2\right)} + \tilde{T}_x \cos\theta + \tilde{T}_y \sin\theta$$
$$\dot{e}_\theta = -u_0 \frac{2 r_d (r + r_p) e_r}{\left(r^2 + r_d^2\right)\left(r^2 + r_p^2\right)} + \frac{1}{r}(-\tilde{T}_x \sin\theta + \tilde{T}_y \cos\theta + \nu_s) \tag{47}$$

The actual and guidance trajectories are defined from the same point, which implies that $r_p(0) = r(0)$ and $\theta_p(0) = \theta(0)$. Consequently, the error signals are zero at the initial time (after the heading convergence to the desired Lyapunov guidance field is achieved).

Remark. It is important to note that we assume throughout this analysis that the desired heading can be obtained before the adaptation process is initialized. In fact, our construction offers some flexibility; the adaptive estimates $\hat{T}_x$ and $\hat{T}_y$ could be initialized in such a way that the desired heading need not be *exactly* achieved. However, via Theorem 2, the exact heading can be achieved provided that the target does not penetrate the initial loiter circle before the correct heading has been obtained.

There are some initial conditions and target trajectories for which the vehicle heading does not converge to the desired heading within a single loiter circle. This situation would arise if a moving target penetrates the initial loiter circle before the desired heading has been obtained. However, because we are assuming that the target moves with constant velocity, the target will eventually exit the initial loiter trajectory. Thus, the desired heading will still be achieved, but it may require more than one initial loiter circle. For simplicity, we assume that we have sufficient initial separation such that the desired heading will be reached within one orbit of the initial loiter circle. As a consequence, the time required for one orbit can be used to initiate the variable airspeed angular spacing control scheme.

B. Stability Analysis

Before commencing the stability analysis, we introduce a smooth parameter projection construction to ensure that the estimates for wind and target motion evolve within the known bounds given by T^*. We define the estimates as follows:

$$\hat{T}_x = T^* \tanh \hat{\phi}_x, \qquad \hat{T}_y = T^* \tanh \hat{\phi}_y \tag{48}$$

where $\hat{\phi}_x$ and $\hat{\phi}_y$ are estimates that can adapt free from any restrictive bounds. The corresponding true parameter values are

$$T_x = T^* \tanh \phi_x^*, \qquad T_y = T^* \tanh \phi_y^* \tag{49}$$

Now consider the Lyapunov function candidate

$$\begin{aligned} V = {} & \tfrac{1}{2}e_r^2 + (\mu/2)e_\theta^2 + (T^*/\gamma)(\log\cosh\hat{\phi}_x - \hat{\phi}_x \tanh\phi_x^*) \\ & + (T^*/\gamma)(\log\cosh\hat{\phi}_y - \hat{\phi}_y \tanh\phi_y^*) + c^* \end{aligned} \tag{50}$$

for any $\mu > 0$ and $\gamma > 0$. The term c^* is a to-be-determined fixed constant to ensure the positive definiteness of V. Evaluating $\dot{V}$ along the trajectories defined by Eq. (47) and defining the adaptive update laws

$$\begin{aligned} \dot{\hat{\phi}}_x &= -\gamma\left[e_r \cos\theta - \mu\frac{e_\theta \sin\theta}{r}\right] \\ \dot{\hat{\phi}}_y &= -\gamma\left[e_r \sin\theta + \mu\frac{e_\theta \cos\theta}{r}\right], \qquad v_s = -\frac{k_\theta u_0}{\gamma}\tanh e_\theta + \beta \end{aligned} \tag{51}$$

for some signal β and constant $k_\theta > 0$, we obtain

$$\begin{aligned} \dot{V} = {} & -u_0 \frac{2r_d^2\left(r^2 - r_p^2\right)e_r^2}{\left(r^2 + r_d^2\right)\left(r^2 + r_p^2\right)} - \frac{k_\theta}{r} e_\theta \tanh e_\theta \\ & - \mu u_0 \frac{2r_d(r + r_p)e_r e_\theta}{\left(r^2 + r_d^2\right)\left(r^2 + r_p^2\right)} + \frac{\mu\beta e_\theta}{r} \end{aligned} \tag{52}$$

The parameter γ has the interpretation of a "learning rate" that governs how fast the adaptation process in Eq. (51) evolves. To cancel the sign-indefinite term in Eq. (52), we choose

$$\beta = \frac{2u_0 r_d(r + r_p)re_r}{\left(r^2 + r_d^2\right)\left(r^2 + r_p^2\right)} \tag{53}$$

and, thus,

$$\dot{V} = -u_0 \frac{2r_d^2\left(r^2 - r_p^2\right)e_r^2}{\left(r^2 + r_d^2\right)\left(r^2 + r_p^2\right)} - \frac{k_\theta u_0}{\gamma r} e_\theta \tanh e_\theta \le 0 \tag{54}$$

provided that $r > 0$, which can be readily established from Eqs. (44) and (48). The constant c^* still remains to be determined. Because the error signals e_r and e_θ are initially zero, and if we set the adaptive estimates $\hat{\phi}_x$ and $\hat{\phi}_y$ to be initially zero, then the third and fourth terms in Eq. (50) have a minimum value whenever $\hat{\phi}_x = \phi_x^*$ and $\hat{\phi}_y = \phi_y^*$. Accordingly, we can define c^* as

$$\begin{aligned} c^* = {} & (T^*/\gamma)[|\log\cosh\phi_x^* - \phi_x^* \tanh\phi_x^*| \\ & + |\log\cosh\phi_y^* - \phi_y^* \tanh\phi_y^*|] \end{aligned} \tag{55}$$

to ensure the positive definiteness of V. Finally, note that c^* is inversely proportional to γ and that $1/2e_r^2(t) \le V(t) \le V(0) = c^*$. This implies $|e_r(t)| \le \sqrt{2c^*}$. From Eq. (55), we establish the following upper bound on c^*:

$$c^* \le \frac{2\log 2T^*}{\gamma} \tag{56}$$

Thus, the maximum radial error from the guidance trajectory can be reduced by increasing the learning rate γ.

C. Kinematic Constraints

There are theoretical and practical limitations to what can be achieved given the kinematic constraints (2) and (3) on the controllers. For example, if either the wind or target speed (or their combined effect) is too large, then it will be impossible to maintain the circular trajectory around the target. Moreover, even when it is possible to maintain the circular trajectory, there may be large demands on airspeed variation that are undesirable or infeasible from a fuel efficiency point of view.

Let us examine the vehicle airspeed command to establish a parameter $\alpha > 0$, such that

$$T^* = \alpha u_0 \tag{57}$$

for the maximum target speed T^* that we can accommodate given the airspeed constraint (2). From Eq. (43), we establish

$$\begin{aligned} u_1^2 = {} & u_0^2 + v_s^2 + \hat{T}_x^2 + \hat{T}_y^2 + 2u_0 v_s \sin\phi \\ & + 2v_s(\hat{T}_y \cos\theta - \hat{T}_x \sin\theta) - 2u_0(\hat{T}_x \cos(\theta - \phi) \\ & + \hat{T}_y \sin(\theta - \phi)) \end{aligned} \tag{58}$$

Using Eqs. (40) and (57), we obtain the following upper bound:

$$u_1^2 \le [|v_s| + u_0(1 + 2\alpha)]^2 \tag{59}$$

To satisfy the airspeed constraint, we require $u_1^2 \le v_{\max}^2$, and so

$$|v_s| \le v_{\max} - u_0(1 + 2\alpha) \tag{60}$$

For Eq. (60) to be meaningful, we need the right-hand side to be positive, which yields an upper bound for α:

$$\alpha < \frac{1}{2}\left[\frac{v_{\max}}{u_0} - 1\right] \tag{61}$$

Next, from Eq. (58), we also establish the following lower bound on the commanded airspeed:

$$u_1^2 \ge |v_s|^2 - 2u_0(1 + 2\alpha)|v_s| + (1 - 4\alpha)u_0^2 \tag{62}$$

To satisfy the airspeed constraint (2), we require $u_1^2 \ge v_{\min}^2$, and so we need

$$|v_s|^2 - 2u_0(1 + 2\alpha)|v_s| + (1 - 4\alpha)u_0^2 - v_{\min}^2 \ge 0 \tag{63}$$

Let r^+ and r^- be the two roots of

$$|v_s|^2 - 2u_0(1 + 2\alpha)|v_s| + (1 - 4\alpha)u_0^2 - v_{\min}^2 = 0 \tag{64}$$

which are given by

$$\begin{aligned} r^+ &= u_0(1 + 2\alpha) + \sqrt{4\alpha^2 u_0^2 + 8\alpha u_0^2 + v_{\min}^2} \\ r^- &= u_0(1 + 2\alpha) - \sqrt{4\alpha^2 u_0^2 + 8\alpha u_0^2 + v_{\min}^2} \end{aligned} \tag{65}$$

Clearly, these are two real, distinct roots with $r^+ > r^-$. Now we can write Eq. (63) as

$$(|v_s| - r^+)(|v_s| - r^-) \geq 0 \tag{66}$$

And to satisfy this, we need $|v_s| \geq r^+$ or $|v_s| \leq r^-$. Because we are interested in upper bounding $|v_s|$, we adopt $|v_s| \leq r^-$, which leads to

$$|v_s| \leq u_0(1 + 2\alpha) - \sqrt{4\alpha^2 u_0^2 + 8\alpha u_0^2 + v_{\min}^2} \tag{67}$$

For Eq. (67) to be meaningful, we need the right-hand side to be positive, which yields a separate upper bound for α given by

$$\alpha < \frac{1}{4}\left[1 - \frac{v_{\min}^2}{u_0^2}\right] \tag{68}$$

Combine Eqs. (61) and (68) to obtain

$$\alpha < \min\left[\frac{1}{2}\left[\frac{v_{\max}}{u_0} - 1\right], \quad \frac{1}{4}\left[1 - \frac{v_{\min}^2}{u_0^2}\right]\right] = \alpha_{\max} \tag{69}$$

to satisfy the airspeed constraint (2). Thus, we have $0 \leq \alpha < \alpha_{\max}$ such that $T^* = \alpha u_0$. From Eq. (69), we can see that there is a tradeoff between the allowable airspeed variation and the maximum allowable wind and target speed: a larger allowable variation in airspeed (i.e., a large $v_{\max}$ and small $v_{\min}$) means that a faster target or stronger wind can be accommodated.

We must also establish a lower bound for the learning rate γ such that the airspeed constraint (2) is satisfied. Because $r = e_r + r_p$ then $|r| \leq |e_r| + |r_p|$. Also, $r_0 \geq |r_p| \geq r_d \; \forall t$ and, as we have already noted, $|e_r| \leq \sqrt{2c^*}$. Then, we obtain the following upper bound on the β term in v_s from Eq. (51) as

$$|\beta| \leq \frac{2u_0\sqrt{2c^*}(\sqrt{2c^*} + r_0)(\sqrt{2c^*} + 2r_0)}{r_d^3} \tag{70}$$

Combining Eqs. (51), (60), (67), and (70), we establish

$$\frac{k_\theta}{\gamma} + \frac{2\sqrt{2c^*}(\sqrt{2c^*} + r_0)(\sqrt{2c^*} + 2r_0)}{r_d^3} \leq \min\left[\frac{v_{\max}}{u_0} - (1 + 2\alpha), (1 + 2\alpha) - \sqrt{4\alpha^2 + 8\alpha + \frac{v_{\min}^2}{u_0^2}}\right] \tag{71}$$

Solving Eq. (71) yields a lower bound for γ, such that if we choose $\gamma > \gamma_{\min}$, then the airspeed constraint will be readily satisfied.

However, we cannot choose an arbitrarily large learning rate γ because there is the potential of violating the heading rate constraint. This can be seen by observing that the heading rate is given by the derivative of Eq. (42), which via Eq. (48) is proportional to the adaptive estimates given in Eq. (51) that are directly scaled by the learning rate γ. Therefore, we must choose an appropriate learning rate γ such that the heading rate constraint is satisfied.

As an example, take $u_0 = 20$ m/s, $r_d = 300$ m, $r_0 = 800$, $k_\theta = 0.001$, $v_{\max} = 25$ m/s, and $v_{\min} = 15$ m/s. Then we have $\alpha_{\max} = 7/64 \approx 0.1095$ and $T^* \approx 2$ m/s, that is, we can accommodate a target speed of approximately one-tenth of the nominal vehicle airspeed u_0. Also, $\gamma_{\min} \approx 202.5$, and so any $\gamma > \gamma_{\min}$ will satisfy the airspeed constraint.

It is important to note that, although the bounds derived in this section are sufficient to guarantee satisfaction of the airspeed constraint, they may not be necessary. Indeed, the process of bounding the various terms is conservative, which is apparent in the simulations that we will report subsequently. In practice, the design choices for the various tradeoffs will ultimately depend on mission particulars and individual UAV capabilities. The controller construction we have proposed allows adjustable parameters to be tuned so that the coordinated standoff tracking objective can be achieved despite uncertainties while also accounting for kinematic constraints.

IV. Information Architectures

In this section, we review some recent developments in formation control that address information architectures using rigid graph theory [2,11,19–23]. We establish a connection between these ideas and the coordinated standoff tracking problem, and thereby associate meaningful information architectures with the decentralized control laws for multiple-vehicle spacing that we present in the following section.

A fundamental task in formation control is to maintain some prescribed geometric shape to keep the vehicles in an optimal sensing configuration. This section is concerned with information architectures required to maintain formation shape. Drawing from a long history in combinatorial theory [24,25], a graph theoretic concept called *rigidity* has recently been proposed to describe information architectures to maintain formation shape [2,19,20]. Roughly speaking, a formation is rigid if it can move as a cohesive whole, with intervehicle distances preserved throughout the motion. This is precisely the goal of the coordinated standoff tracking problem: we desire all vehicles to maintain a standoff distance from the target and an angular spacing from one another. Not every intervehicle distance must be maintained; if enough well-chosen distances are actively kept constant, the rest will be held constant as a consequence. This allows the construction of decentralized control laws based on rigid information architectures.

It is possible to control a particular intervehicle distance in two ways: 1) assign the responsibility to both vehicles, that is, both vehicles actively maintain the distance, and 2) assign the responsibility to only one of the vehicles, that is, one vehicle actively maintains the distance whereas the other does nothing to maintain that particular distance. This distinction gives rise to two types of information architectures: symmetric and asymmetric, respectively. Symmetric information architectures are modeled by an undirected graph, whereas asymmetric information architectures are modeled with a directed graph.

A. Symmetric Information Architecture Rigidity

A graph $G(V, E)$, where V is a set of vertices and $E \in V \times V$ is a set of edges, provides a useful high-level model of the information architecture. We denote a formation $F(G, p)$ where G is the information architecture graph and p: $V \to \Re^{2|V|}$ is a mapping that assigns a position in the plane to each vertex. The vertices represent vehicles, and the edges represent information flow amongst the vehicles. An edge is present between two vertices whenever the distance between the two vehicles is actively maintained. If a vertex j is connected by an edge to vertex i, we call j a *neighbor* of i. The distance is maintained using control laws to govern the motion of each vehicle. The control law for each vehicle requires the relative positions of its neighbors in an arbitrary local coordinate basis.

Consider the rigidity function f: $\Re^{d|V|} \to \Re^{|E|}$ defined by

$$f(p) = [\ldots, \|(pi - pj)\|^2, \ldots] \tag{72}$$

where the kth entry of f corresponds to the squared distance between vertices i and j when they are connected by an edge. Now suppose that the formation moves but $f(p)$ stays constant, that is, the edges in E correspond to links where distance is preserved. Then, expanding about the constant value in a Taylor series and ignoring higher-order terms, we obtain

$$J_f(p)\delta p = 0 \tag{73}$$

where δp is an infinitesimal perturbation of the formation and $J_f(p)$ is the Jacobian of f. This Jacobian is known as the *rigidity matrix* $R(p)$. Equivalently, we obtain

$$J_f(p)\dot{p} = 0 \tag{74}$$

for a formation undergoing smooth motion. When the formation is rigid, the only permissible smooth motions are translation or rotation of the whole formation. In the plane, this accounts for three linearly independent vectors, and so the kernel of $J_f(p)$ has a dimension of

three. This leads us to the following linear algebraic characterization of rigidity [26].

Theorem 3. A formation $F(G, p)$ is rigid if and only if rank $[R(p)] = 2|V| - 3$, which is the maximum rank $R(p)$ can have.

Because the rigidity matrix is a Jacobian of a rational function, it has the same rank for all points but a set of Lebesgue measure zero (via a nontrivial result of Sard [27]), corresponding to special vehicle configurations (e.g., there is a set of collinear or collocated vehicles) that cause the rank deficiency. This leads to the notion of *generic* rigidity. For generic configurations (when the special configurations are precluded), information about formation rigidity is contained in the graph, which allows for a purely combinatorial characterization of rigidity. The result is given by the celebrated Laman's theorem [28]:

Theorem 4. A graph $G(V, E)$ in the plane is rigid if and only if there exists a subset E' of edges such that the induced subgraph $G'(V, E')$ satisfies the following:

1) $|E'| = 2|V| - 3$.

2) Any subgraph $G''(V'', E'')$ of G' with at least two vertices satisfies $|E''| \leq 2|V''| - 3$.

A graph is called *minimally rigid* if it is rigid and there exists no rigid graph with the same number of vertices and a smaller number of edges. Equivalently, a graph is *minimally rigid* if removing any edge results in loss of rigidity. The minimum number of required edges is linear in the number of vehicles. In contrast, in an all-to-all information architecture (i.e., every intervehicle distance is actively maintained), the number of required edges is quadratic in the number of vehicles. Figure 7 illustrates nonrigid, minimally rigid, and nonminimally rigid formations with four vertices [11].

B. Asymmetric Information Architecture Persistence

An asymmetric information architecture is modeled by a directed graph in which a direction is assigned to every edge with an outward arrow from the vehicle responsible for controlling the intervehicle distance. Because only one vehicle is responsible for controlling a particular intervehicle distance, the overall information complexity is reduced by half. This structure minimizes the number of information links and may be necessary when there are limitations on sensor range. In this case, rigidity is necessary, but not sufficient, to preserve all intervehicle distances in a formation with a directed graph. A further concept called *constraint consistence* is needed to generalize the notion of rigidity to directed graphs. To distinguish this notion from rigidity, it is called *persistence*. A graph is called *minimally persistent* if it is both minimally rigid and constraint consistent. In practical terms, constraint consistence rules out certain information flow patterns that make it impossible to maintain formation shape, as illustrated in Fig. 8 [11].

The following two key results are relevant in the plane [11].

Theorem 5. Any directed graph in the plane with no vertex having more than two outgoing edges is constraint consistent.

Theorem 6. A directed graph in the plane is minimally persistent if and only if it is minimally rigid and constraint consistent.

A special case of a persistent information architecture is a "leader–follower" structure in which one vehicle can move freely in the plane and the remaining vehicles maintain a shape around the leader [22]. The structure of the coordinated standoff tracking problem is naturally leader–follower: the target is the leader because it is not constrained to maintain any relative distances, and the engaging

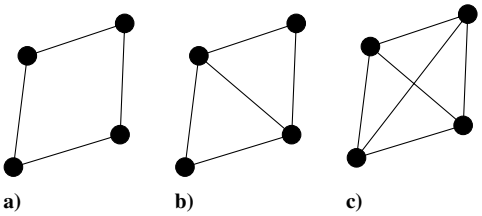

Fig. 7 Illustration of the formations: a) nonrigid, b) minimally rigid, and c) nonminimally rigid.

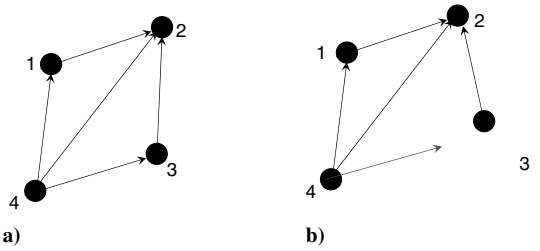

Fig. 8 Illustration of constraint consistence. Vehicle 4 must maintain its distance from vehicles 1, 2, and 3. However, because vehicle 3 must only maintain its distance from vehicle 2, it is free to move in a circle around vehicle 2. Supposing that vehicles 1 and 2 remain stationary and vehicle 3 can move as described, it is impossible for vehicle 4 to maintain all constraints. Note that the underlying undirected graph is rigid.

vehicles are followers that maintain their distances to the target and to one another.

Remark. There is an important distinction to be made between decentralized design and decentralized implementation. Rigidity and persistence are inherently centralized properties of the formation in that it is impossible for a single vehicle to guarantee rigidity of the whole formation. Therefore, rigid and persistent information architectures represent centralized *design* techniques. However, these architectures provide a basis for the design of control laws that have decentralized *implementation*. Once the architecture is established, the implementation of the design is decentralized in that the vehicles can operate using only local information.

V. Stationary Target Tracking: Multiple-Vehicle Spacing

This section develops decentralized control laws to achieve desired angular spacing when multiple vehicles engage a stationary target. We consider two different information architectures based on the structures referred to in the previous section. The first architecture is asymmetric minimally persistent leader–follower. The second architecture is nonminimally persistent leader–follower with a symmetric structure on the engaging vehicles. For both architectures, we show global asymptotic stability of the desired formation.

Each vehicle uses a variable airspeed controller to obtain the desired spacing. We explicitly account for the airspeed constraint (2) by introducing a design variable that adjusts the amount of allowable airspeed variation without diluting our convergence properties. In this way, the fuel expenditure required to obtain the desired angular spacing can be minimized. There is a tradeoff: a larger allowable airspeed variation means faster convergence and a smaller allowable airspeed variation means slower convergence.

The angular spacing control commences once all of the UAVs complete their initial respective loiter arcs. The required time for all the vehicles to match headings with the guidance field is analytically determined from only the knowledge of the initial conditions of all the vehicles when there is no wind or target motion; in the case with wind and target motion, the time can be upper bounded according to Theorem 2 by the time required to execute a loiter circle. Accordingly, we assume in this section that, without loss of generality, all the vehicles have already matched their heading with the guidance field.

In the following subsections, we develop control laws based on a minimally persistent leader–follower information architecture. The target is the leader because it does not maintain any distances to the engaging UAVs. One of the engaging UAVs maintains the circular orbit around the target and has no other distances to maintain. The remaining vehicles maintain the circular orbit around the target and, through adjustments in airspeed, maintain a prescribed angular spacing with the neighboring vehicle ahead of it in the circular orbit. This structure requires the minimum possible number of communication/sensing links to achieve the circular orbit and angular spacing.

A. Control Laws and Stability Analysis

The dynamics for the ith vehicle in polar coordinates are given by

$$\dot{r}_i = -u_{1i}\frac{r_i^2 - r_d^2}{r_i^2 + r_d^2} \tag{75}$$

$$r_i\dot{\theta}_i = u_{1i}\frac{2r_i r_d}{r_i^2 + r_d^2}, \qquad i = 1, \ldots, n \tag{76}$$

We designate vehicle n to have a constant airspeed:

$$u_{1n} = u_0 \tag{77}$$

Let the airspeed input of the remaining $n-1$ vehicles be given by

$$u_{1i} = u_0 + \Delta V_{\max}\tanh(\theta_{i+1} - \theta - \theta_d)\frac{r_i^2 + r_d^2}{r_{i+1}^2 + r_i^2} \tag{78}$$

where $\Delta V_{\max} > 0$ is a design parameter to be chosen such that Eq. (78) satisfies the airspeed constraint and θ_d is the desired angular spacing between each pair of vehicles. To satisfy the airspeed constraint, we require $u_0 - \Delta V_{\max} > v_{\min} > 0$. When the angular spacing is different from what is desired, the second term adjusts the airspeed to compensate. When the desired spacing is achieved, the second term goes to zero and the airspeed becomes the constant nominal u_0. We emphasize that any positive value for $\Delta V_{\max}$ is sufficient to achieve the desired spacing. Therefore, the amount of allowable airspeed variation can be adjusted to maximize fuel efficiency. The tradeoff for choosing a small $\Delta V_{\max}$ is that convergence to the desired angular spacing may be slower.

We define the angular spacing errors as $\delta\theta_i = \theta_{i+1} - \theta_i - \theta_d$. We then differentiate and use Eq. (75) with Eq. (78) to obtain angular spacing error dynamics as

$$\begin{aligned}
\delta\dot{\theta}_{n-1} &= \frac{2u_0 r_d\left(r_{n-1}^2 - r_n^2\right)}{\left(r_n^2 + r_d^2\right)\left(r_{n-1}^2 + r_d^2\right)} \\
&\quad - \frac{2r_d\Delta V_{\max}}{\left(r_n^2 + r_{n-1}^2\right)}\tanh(\delta\theta_{n-1}), \qquad i = n-1 \\
\delta\dot{\theta}_i &= \frac{2u_0 r_d\left(r_i^2 - r_{i+1}^2\right)}{\left(r_{i+1}^2 + r_d^2\right)\left(r_i^2 + r_d^2\right)} + \frac{2r_d\Delta V_{\max}}{\left(r_{i+2}^2 + r_{i+1}^2\right)}\tanh(\delta\theta_{i+1}) \\
&\quad - \frac{2r_d\Delta V_{\max}}{\left(r_{i+1}^2 + r_i^2\right)}\tanh(\delta\theta_i), \qquad i = 1, \ldots, n-2
\end{aligned} \tag{79}$$

Now consider the Lyapunov function candidate

$$V = \sum_{i=1}^{n-1}\log\cosh\delta\theta_i + \frac{1}{2}\sum_{i=1}^{n}\lambda_i r_i^2 \tag{80}$$

with some suitably chosen $\lambda_i > 0$. Evaluating $\dot{V}$ along the trajectories defined by Eqs. (75) and (79), we obtain

$$\begin{aligned}
\dot{V} &= \sum_{i=1}^{n-1}\left[\frac{2u_0 r_d\left(r_i^2 - r_{i+1}^2\right)}{\left(r_{i+1}^2 + r_d^2\right)\left(r_i^2 + r_d^2\right)}\tanh(\delta\theta_i)\right. \\
&\quad \left. - \frac{2r_d\Delta V_{\max}}{\left(r_{i+1}^2 + r_i^2\right)}\tanh^2(\delta\theta_i) - \lambda_i r_i u_{1i}\frac{r_i^2 - r_d^2}{r_i^2 + r_d^2}\right] \\
&\quad + \sum_{i=1}^{n-2}\left[\frac{2r_d\Delta V_{\max}}{\left(r_{i+2}^2 + r_{i+1}^2\right)}\tanh(\delta\theta_{i+1})\tanh(\delta\theta_i)\right] \\
&\quad - \lambda_n r_n u_0\frac{r_n^2 - r_d^2}{r_n^2 + r_d^2}
\end{aligned} \tag{81}$$

Using the fact that $r_d \le r_i(t) \le r_{i0}$ from Eq. (75) and $u_{12} \ge u_0 - \Delta V_{\max}$ from Eq. (78), we can bound $\dot{V}$ as

$$\begin{aligned}
\dot{V} &\le \sum_{i=1}^{n-1}\left[-\frac{\Delta V_{\max} r_d}{\bar{r}_0^2}\tanh^2\delta\theta_i + \frac{u_0\left(r_i^2 - r_d^2\right)}{r_d\left(r_i^2 + r_d^2\right)} + \frac{u_0\left(r_{i+1}^2 - r_d^2\right)}{r_d\left(r_{i+1}^2 + r_d^2\right)}\right. \\
&\quad \left. - \lambda_i r_d(u_0 - \Delta V_{\max})\frac{\left(r_i^2 - r_d^2\right)}{\left(r_i^2 + r_d^2\right)}\right] \\
&\quad + \sum_{i=1}^{n-2}\left[\frac{\Delta V_{\max}}{r_d}\tanh(\delta\theta_{i+1})\tanh(\delta\theta_i)\right] - \lambda_n r_n u_0\frac{r_n^2 - r_d^2}{r_n^2 + r_d^2}
\end{aligned} \tag{82}$$

We can rewrite it as

$$\begin{aligned}
\dot{V} &\le -\tanh\delta\theta^T C\tanh\delta\theta \\
&\quad - \sum_{i=1}^{n-1}\left[\left[\lambda_i r_d(u_0 - \Delta V_{\max}) - \frac{2u_0}{r_d}\right]\frac{\left(r_i^2 - r_d^2\right)}{\left(r_i^2 + r_d^2\right)}\right] \\
&\quad - \left(\lambda_n r_n u_0 - \frac{u_0}{r_d}\right)\frac{\left(r_i^2 - r_d^2\right)}{\left(r_i^2 + r_d^2\right)}
\end{aligned} \tag{83}$$

where $\tanh\delta\theta = [\tanh(\delta\theta_1), \ldots, \tanh(\delta\theta_{n-1})]$ and the matrix C has the positive-definite structure

$$C = \begin{bmatrix}
\frac{\Delta V_{\max} r_d}{\bar{r}_0^2} & -\frac{\Delta V_{\max}}{r_d} & 0 & \cdots & 0 \\
0 & \frac{\Delta V_{\max} r_d}{\bar{r}_0^2} & -\frac{\Delta V_{\max}}{r_d} & \cdots & 0 \\
0 & \cdots & \ddots & \cdots & 0 \\
0 & \cdots & 0 & \frac{\Delta V_{\max} r_d}{\bar{r}_0^2} & -\frac{\Delta V_{\max}}{r_d} \\
0 & 0 & \cdots & 0 & \frac{\Delta V_{\max} r_d}{\bar{r}_0^2}
\end{bmatrix} \tag{84}$$

Choosing

$$\begin{aligned}
\lambda_n &> \left(1/r_d^2\right) \\
\lambda_i &> \left(u_0/r_d^2\right)(u_0 - \Delta V_{\max}), \qquad i = 1, \ldots, n-1
\end{aligned} \tag{85}$$

we obtain $\dot{V} \le 0$. This implies

$$\lim_{t\to\infty} r_i(t) = r_d, \quad \forall\ i \tag{86}$$

which achieves the circular standoff radius, and

$$\lim_{t\to\infty}\delta\theta_i(t) = 0, \quad \forall\ i \tag{87}$$

which achieves the angular spacing objective.

B. Nonminimally Persistent Information Architecture

In this subsection we develop control laws based on a nonminimally persistent information architecture with a symmetric structure for the engaging UAVs. The airspeed is adjusted such that each vehicle moves toward the midpoint of its two nearest neighbors on the circle. Although this structure does not contain the minimum possible number of information links, it has the advantage that the vehicles do not need to know the number of engaging vehicles.

1. *Control Laws and Stability Analysis*

The vehicles each have dynamics given by Eq. (75). Let the airspeed command for the ith vehicle be given by

$$u_{1i} = u_0 - \Delta V_{\max}\tanh\delta\theta_i\frac{r_i^2 + r_d}{r_{i-1}^2 + r_i^2 + r_{i+1}^2} \tag{88}$$

where $\Delta V_{\max} > 0$ is a design parameter chosen such that the input satisfies the airspeed constraint. Again, any positive value for the parameter $\Delta V_{\max}$ is sufficient to achieve the desired spacing, and so the amount of allowable airspeed variation can be adjusted to maximize fuel efficiency. The ith angular spacing error is given by

$$\delta\theta_i = \theta_i - \tfrac{1}{2}(\theta_{i-1} + \theta_{i+1}) \tag{89}$$

where a modulo n cycle is formed around the circle

$$\theta_0 = \theta_n - 2\pi, \qquad \theta_{n+1} = \theta_1 + 2\pi \tag{90}$$

Differentiating Eq. (89), we obtain

$$\begin{aligned}\delta\dot{\theta}_i = {} & -\Delta V_{\max}\frac{r_d}{R_i^2}(2\tanh(\delta\theta_i) + \tanh(\delta\theta_{i+1}) + \tanh(\delta\theta_{i-1})) \\ & + \frac{r_d u_0\left(r_{i+1}^2 - r_d^2\right)}{\left(r_i^2 + r_d^2\right)\left(r_{i+1}^2 + r_d^2\right)} + \frac{r_d u_0\left(r_{i-1}^2 - r_d^2\right)}{\left(r_i^2 + r_d^2\right)\left(r_{i-1}^2 + r_d^2\right)} \\ & - \frac{r_d u_0\left(r_i^2 - r_d^2\right)}{\left(r_i^2 + r_d^2\right)\left(r_{i+1}^2 + r_d^2\right)} - \frac{r_d u_0\left(r_i^2 - r_d^2\right)}{\left(r_i^2 + r_d^2\right)\left(r_{i-1}^2 + r_d^2\right)}\end{aligned} \tag{91}$$

where

$$R_i^2 = \sum_{j-1}^{j+1} r_j^2$$

Consider the Lyapunov function candidate

$$V = \sum_{i=1}^{n}\left[\log\cosh(\delta\theta_i) + \frac{\lambda}{2}r_i^2\right] \tag{92}$$

for some $\lambda > 0$. Evaluating $\dot{V}$ along Eqs. (75) and (91), and again using the fact that $r_d \le r_i(t) \le r_{i0}$ from Eq. (75) and $u_{12} \ge u_0 - \Delta V_{\max}$ from Eq. (78), we can bound $\dot{V}$ as

$$\begin{aligned}\dot{V} \le {} & -\frac{\Delta V_{\max} r_d}{R_i^2}[(|\tanh\delta\theta_1| - |\tanh\delta\theta_2|)^2 \\ & + (|\tanh\delta\theta_2| - |\tanh\delta\theta_3|)^2 + \cdots + (|\tanh\delta\theta_{n-1}| \\ & - |\tanh\delta\theta_n|)^2 + (|\tanh\delta\theta_n| - |\tanh\delta\theta_1|)^2] \\ & + \sum_{i=1}^{n}\left[\frac{2u_0}{r_d} - \lambda r_d(u_0 - \Delta V_{\max})\right]\frac{r_i^2 - r_d^2}{r_i^2 + r_d^2}\end{aligned} \tag{93}$$

Choosing

$$\lambda > \frac{2u_0}{r_d^2(u_0 - \Delta V_{\max})} \tag{94}$$

we have $\dot{V} \le 0$. This implies

$$\lim_{t\to\infty}|\tanh\delta\theta_i| = \bar{T} \quad \forall\ i \tag{95}$$

where $\bar{T}$ is a finite constant. Thus, $\delta\theta_i = \bar{\theta}\ \forall i$ as $t \to \infty$ where $\bar{\theta}$ is a finite constant.

Now we define the angle differences

$$e_{12} = \theta_1 - \theta_2 \qquad e_{23} = \theta_2 - \theta_3 \qquad \vdots \qquad e_{n-1,n} = \theta_{n-1} - \theta_n$$
$$e_{n1} = \theta_n - \theta_1 \tag{96}$$

and, in the limit as $t \to \infty$, we obtain from Eqs. (89) and (96) the following relationship between the angular spacing errors and the angle differences:

$$\begin{aligned}\begin{bmatrix}\delta\theta_1\\ \delta\theta_2\\ \delta\theta_3\\ \vdots\\ \delta\theta_{n-1}\\ \delta\theta_n\end{bmatrix} &= \begin{bmatrix}\bar{\theta}\\ \bar{\theta}\\ \bar{\theta}\\ \vdots\\ \bar{\theta}\\ \bar{\theta}\end{bmatrix} \\ &= \begin{bmatrix}\frac{1}{2} & 0 & 0 & \cdots & 0 & -\frac{1}{2}\\ -\frac{1}{2} & \frac{1}{2} & 0 & 0 & \cdots & 0\\ 0 & -\frac{1}{2} & \frac{1}{2} & 0 & \cdots & 0\\ \vdots & \cdots & \ddots & \ddots & 0 & 0\\ 0 & \cdots & 0 & -\frac{1}{2} & \frac{1}{2} & 0\\ 0 & 0 & \cdots & 0 & -\frac{1}{2} & \frac{1}{2}\end{bmatrix}\begin{bmatrix}e_{12}\\ e_{23}\\ e_{34}\\ \vdots\\ e_{n-1,n}\\ e_{n1}\end{bmatrix} + \begin{bmatrix}\pi\\ 0\\ 0\\ \vdots\\ 0\\ -\pi\end{bmatrix}\end{aligned} \tag{97}$$

Further, observe that the sum of all angle differences is zero:

$$e_{12} + e_{23} + e_{34} + \cdots + e_{n-1,n} + e_{n1} = 0 \tag{98}$$

This gives $n + 1$ equations in $n + 1$ unknowns (n angle differences and $\bar{\theta}$). Solving, we obtain $\bar{\theta} = 0$ and

$$e_{ij} = (2\pi/n)\ \forall i, j \tag{99}$$

and equal angular spacing is achieved in the limit as $t \to \infty$.

VI. Simulations

In this section, we present simulations to demonstrate our control laws for the coordinated standoff tracking problem. We only show simulations for the minimally persistent information architecture. The nonminimally persistent information architecture exhibits the same qualitative behavior; accordingly, we do not include the associated simulation results. We present simulations for four UAVs engaging a stationary target and two UAVs engaging a moving target.

Figure 9 shows four UAVs engaging a stationary target with $u_0 = 20$ m/s, $r_d = 300$ m, $\Delta V_{\max} = 5$ m/s, $x_{10} = 1000$ m, $y_{10} = 1000$ m, $\psi_{10} = 0$, $x_{20} = -800$ m, $y_{20} = -700$ m, $\psi_{20} = \pi/2$, $x_{30} = -500$ m, $y_{30} = 900$ m, $\psi_{30} = \pi$, $x_{40} = 700$ m, $y_{40} = -100$ m, and $\psi_{40} = -\pi/4$. The vehicles initially have arbitrary headings and execute the initial loiter circle to converge to the desired heading along the Lyapunov guidance vector field. When all vehicles arrive within a prescribed distance from the standoff radius, the variable airspeed controllers commence to achieve the desired angular spacing. The airspeed commands are shown in Fig. 10. The airspeed of the first follower remains constant whereas the other vehicles adjust their airspeeds to achieve the spacing. The relative spacing errors (we show relative distances here, which are equivalent

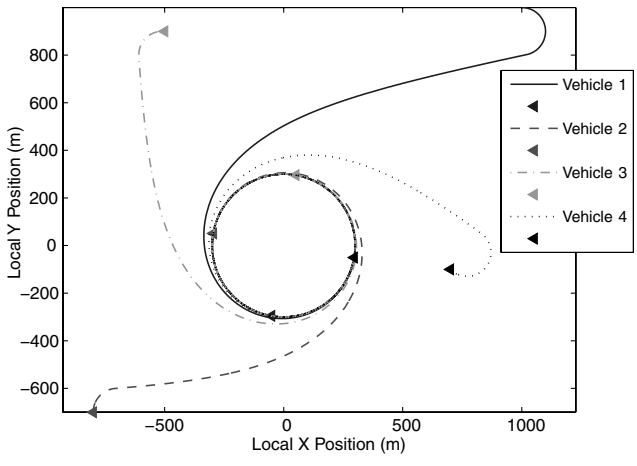

Fig. 9 Four UAVs engaging a stationary target in local coordinates.

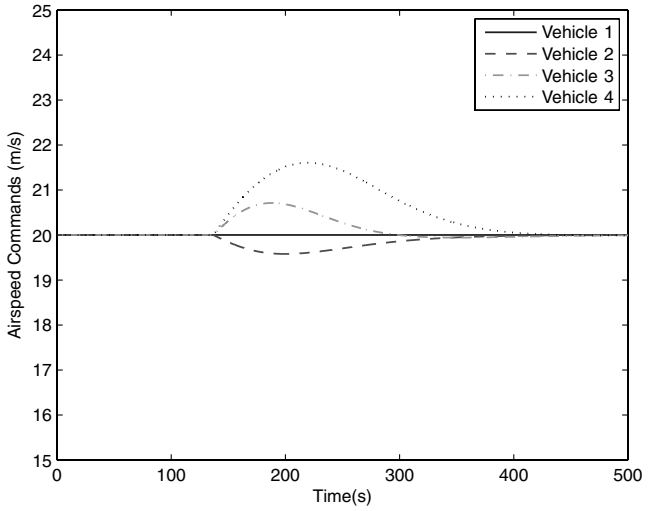

Fig. 10 Airspeed commands for spacing.

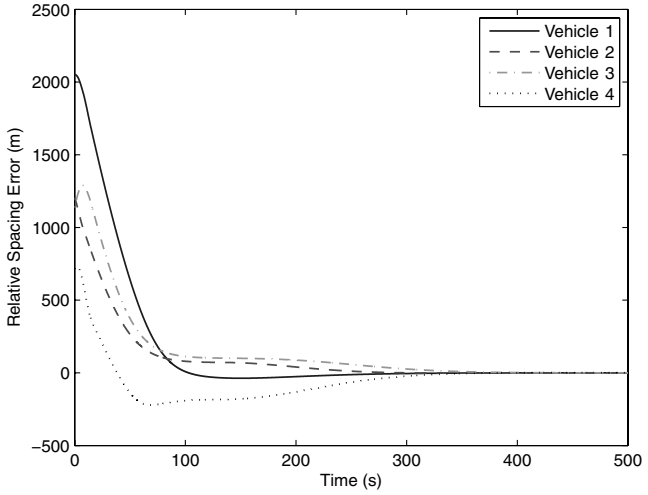

Fig. 11 Relative spacing errors for four UAVs engaging a stationary target.

to relative angles in this case) are shown in Fig. 11 and all converge to zero.

Figure 12 shows two UAVs engaging a target moving with constant velocity in inertial coordinates where $u_0 = 20$ m/s, $r_d = 400$ m, $\Delta V_{\max} = 5$ m/s, $\gamma = 0.01$, $\mu = 1$, $k_\theta = 0.01$, $x_{10} = 1100$ m, $y_{10} = 800$ m, $\psi_{10} = 0$, $x_{20} = 800$ m, $y_{20} = -800$ m, $\psi_{20} = 0$, $T_x = 3$ m/s, and $T_y = 3$ m/s. The target speeds T_x and T_y and the learning rate γ are outside the range of values established in our analysis in Sec. III. Despite this, the vehicles accomplish the coordinated standoff tracking objectives, which highlights the conservatism inherent in the various upper bounds that were derived. The vehicles again initially have arbitrary headings and execute the same initial loiter circle at a constant airspeed to converge to the desired heading. When the desired heading is achieved, the variable airspeed control commences, which adapts for the unknown wind and target motion. After a prescribed time, the variable airspeed angular spacing control commences for the vehicles to obtain a prescribed angular separation of π. The trajectories are shown in local target frame coordinates in Fig. 13, in which it is readily seen that the circular orbit pattern is achieved despite the unknown wind and target motion. The airspeed commands for spacing and maintaining the circular orbit are shown in Fig. 14, and the variations are within 25% of the nominal airspeed. The relative spacing error (we show the relative distance here, which is equivalent to the relative angle in this case) is shown in Fig. 15 and converges to zero.

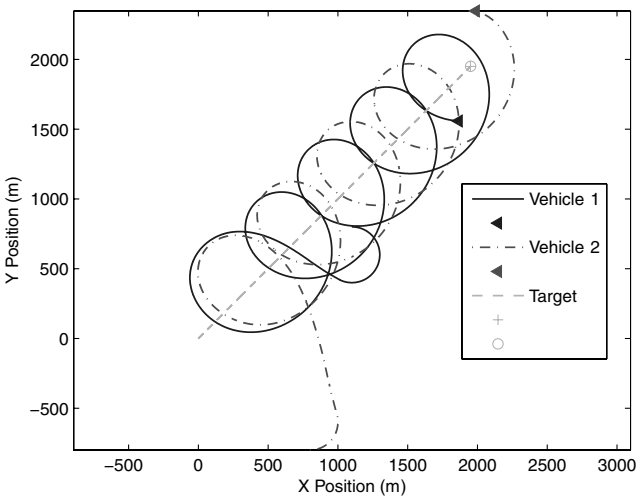

Fig. 12 Two UAVs engaging a moving target in inertial coordinates.

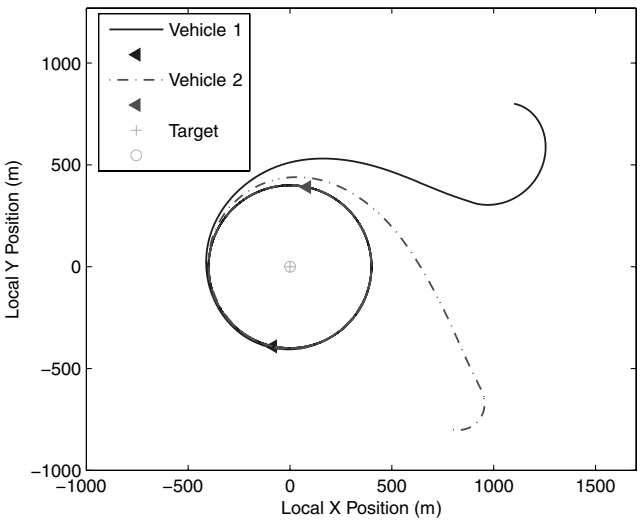

Fig. 13 Two UAVs engaging a moving target in local target frame coordinates.

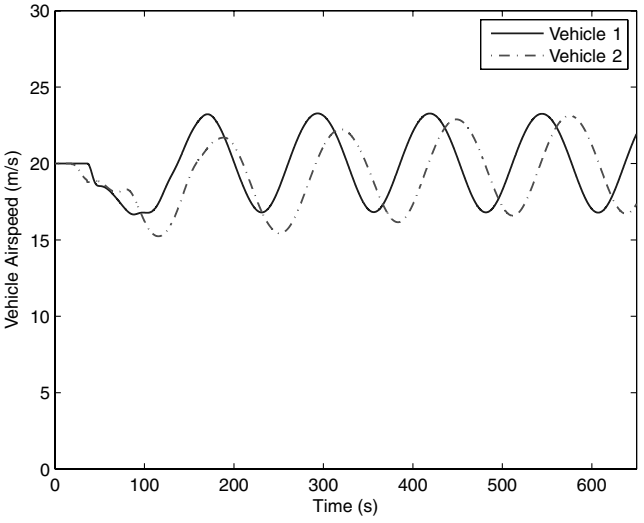

Fig. 14 Airspeed commands for spacing and maintaining circular orbit around a moving target.

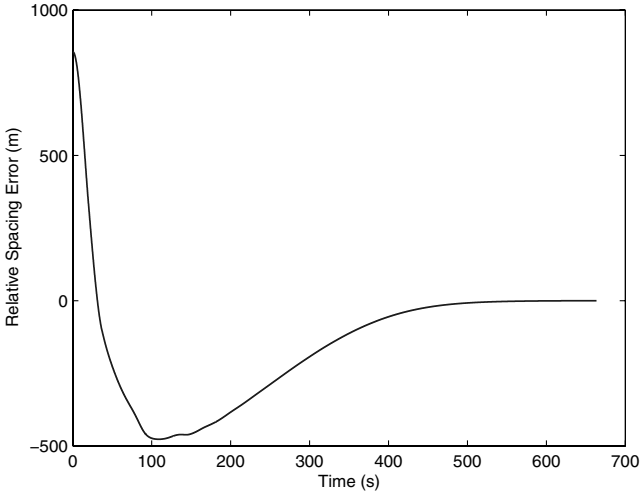

Fig. 15 Relative spacing error for two UAVs engaging a moving target.

VII. Conclusions

This paper has further developed the Lyapunov guidance vector field approach to the coordinated standoff tracking problem. For single-vehicle path planning, we presented a proof of heading convergence that addresses a previously neglected timescale separation issue. We then proposed a novel approach for heading convergence that uses an analytical solution to the guidance vector field and offers theoretical and practical advantages. We also extended the approach to accommodate unknown target motion and wind by introducing adaptive estimates to ensure stability of the circular trajectory. For multiple-vehicle coordination, a variable airspeed controller was implemented to achieve the prescribed intervehicle angular spacing. We established a connection with recent work in information architectures modeled by rigid graph theory and based our control laws on two separate architectures that were derived from that theory. We showed that the desired formation is globally asymptotically stable.

There are many potential directions for future consideration. First, one could consider a more detailed model for vehicle dynamics that evolves in three dimensions and includes inertial effects and attitude dynamics. Second, the adaptive control techniques could be extended to encompass a more general target motion. Third, the results in the paper are suitable for implementation on an experimental testbed. It would be interesting to identify specific aspects of the current theory that are most in need of generalization. Finally, the connection between the development of decentralized control laws and the graph theoretic models of the information architecture motivates a study of more general information architectures. An ultimate goal is the establishment of a general framework for the cooperative control of autonomous vehicle formations in which decentralized control laws for a variety of tasks can be designed based on scalable and meaningful information architectures.

Acknowledgments

This research was conducted as part of the American Society for Engineering Education–U.S. Air Force Office of Scientific Research Summer Faculty Fellowship Program and the U.S. Air Force Research Laboratory Air Vehicles Directorate Summer Research Program. The authors would like to thank Karl Obermeyer of the University of California, Santa Barbara, for his helpful discussions and suggestions.

References

[1] Chandler, P., Pachter, M., and Rasmussen, S., "UAV Cooperative Control," *Proceedings of the American Control Conference*, Vol. 1, IEEE Publications, Piscataway, NJ, 2001, pp. 50–55. doi:10.1109/ACC.2001.945512

[2] Olfati-Saber, R., and Murray, R., "Graph Rigidity and Distributed Formation Stabilization of Multi-Vehicle Systems," *Proceedings of the 41st IEEE Conference on Decision and Control*, Vol. 3, IEEE Publications, Piscataway, NJ, 2002.

[3] Fax, J., and Murray, R., "Information Flow and Cooperative Control of Vehicle Formations," *IEEE Transactions on Automatic Control*, Vol. 49, No. 9, 2004, pp. 1465–1476. doi:10.1109/TAC.2004.834433

[4] Ogren, P., Fiorelli, E., and Leonard, N., "Cooperative Control of Mobile Sensor Networks: Adaptive Gradient Climbing in a Distributed Environment," *IEEE Transactions on Automatic Control*, Vol. 49, No. 8, 2004, pp. 1292–1302. doi:10.1109/TAC.2004.832203

[5] Lin, Z., Broucke, M., and Francis, B., "Local Control Strategies for Groups of Mobile Autonomous Agents," *IEEE Transactions on Automatic Control*, Vol. 49, No. 4, 2004, pp. 622–629. doi:10.1109/TAC.2004.825639

[6] Ren, W., and Beard, R., "Decentralized Scheme for Spacecraft Formation Flying via the Virtual Structure Approach," *Journal of Guidance, Control, and Dynamics*, Vol. 27, No. 1, 2004, pp. 73–82. doi:10.2514/1.9287

[7] Gu, G., Chandler, P., Schumacher, C., Sparks, A., and Pachter, M., "Optimal Cooperative Sensing Using a Team of UAVs," *IEEE Transactions on Aerospace and Electronic Systems*, Vol. 42, No. 4, 2006, pp. 1446–1458. doi:10.1109/TAES.2006.314584

[8] Gerla, M., and Xu, K., "Integrating Mobile Swarms with Large-Scale Sensor Networks Using Satellites," *IEEE 59th Vehicular Technology Conference*, Vol. 5, IEEE Publications, Piscataway, NJ, 2004, pp. 2816–2820. doi:10.1109/VETECS.2004.1391436

[9] Sepulchre, R., Paley, D., and Leonard, N., "Stabilization of Planar Collective Motion: All-to-All Communication," *IEEE Transactions on Automatic Control*, Vol. 52, No. 5, 2007, pp. 811–824. doi:10.1109/TAC.2007.898077

[10] Sepulchre, R., Paley, D., and Leonard, N., "Stabilization of Planar Collective Motion with Limited Communication," *IEEE Transactions on Automatic Control*, Vol. 53, No. 3, 2008, pp. 706–719. doi:10.1109/TAC.2008.919857

[11] Anderson, B., Yu, C., Fidan, B., and Hendrickx, J., "Control and Information Architectures for Autonomous Formations," *IEEE Control Systems Magazine* (to be published).

[12] Ioannou, P., "Decentralized Adaptive Control of Interconnected Systems," *IEEE Transactions on Automatic Control*, Vol. 31, No. 4, 1986, pp. 291–298. doi:10.1109/TAC.1986.1104282

[13] Martínez, S., and Bullo, F., "Optimal Sensor Placement and Motion Coordination for Target Tracking," *Automatica*, Vol. 42, No. 4, 2006, pp. 661–668. doi:10.1016/j.automatica.2005.12.018

[14] Frew, E., and Lawrence, D., "Cooperative Standoff Tracking of Moving Targets Using Lyapunov Guidance Vector Fields," *Journal of Guidance, Control, and Dynamics*, Vol. 31, No. 2, 2008, pp. 290–306. doi:10.2514/1.30507

[15] Kingston, D., and Beard, R., "UAV Splay State Configuration for Moving Targets in Wind," Lecture Notes in Control and Information Sciences, Vol. 369, edited by M. Thoma and M. Morari, Springer, New York, 2007, pp. 109–128.

[16] Marshall, J., Broucke, M., and Francis, B., "Pursuit Formations of Unicycles," *Automatica*, Vol. 42, No. 1, 2006, pp. 3–12. doi:10.1016/j.automatica.2005.08.001

[17] Savla, K., Bullo, F., and Frazzoli, E., "On Traveling Salesperson Problems for Dubins Vehicle: Stochastic and Dynamic Environments," *44th IEEE Conference on Decision and Control*, IEEE Publications, Piscataway, NJ, 2005, pp. 4530–4535.

[18] Griffiths, S., "Vector Field Approach for Curved Path Following for Miniature Aerial Vehicles," *Proceedings of the AIAA Guidance, Navigation, and Control Conference*, Vol. 61, AIAA, Reston, VA, 2006, pp. 63–64.

[19] Eren, T., Belhumeur, P., Anderson, B., and Morse, A., "A Framework for Maintaining Formations Based on Rigidity," *Proceedings of the 15th IFAC World Congress*, Elsevier, Oxford, 2002, pp. 2752–2757.

[20] Baillieul, J., and Suri, A., "Information Patterns and Hedging Brockett's Theorem in Controlling Vehicle Formations," *Proceedings of the 42nd IEEE Conference on Decision and Control*, Vol. 1, IEEE Publications, Piscataway, NJ, 2003, pp. 556–563. doi:10.1109/CDC.2003.1272622

[21] Eren, T., Anderson, B., Morse, A., Whiteley, W., and Belhumeur, P., "Operations on Rigid Formations of Autonomous Agents," *Communications in Information and Systems*, Vol. 3, No. 4, 2004, pp. 223–258.

[22] Yu, C., Hendrickx, J., Fidan, B., Anderson, B., and Blondel, V., "Three and Higher Dimensional Autonomous Formations: Rigidity, Persistence and Structural Persistence," *Automatica*, Vol. 43, No. 3, 2007, pp. 387–402. doi:10.1016/j.automatica.2006.08.025

[23] Fidan, B., Yu, C., and Anderson, B., "Acquiring and Maintaining Persistence of Autonomous Multi-Vehicle Formations," *IET Control Theory & Applications*, Vol. 1, No. 2, 2007, pp. 452–460. doi:10.1049/iet-cta:20050409

[24] Henneberg, L., *Die Graphische Statik der Starren Systeme*, B.G. Teubner, Stuttgart Germany, 1911.

[25] Tay, T., and Whiteley, W., "Generating Isostatic Frameworks," *Structural Topology*, Vol. 11, 1985, pp. 21–69.

[26] Asimow, L., and Roth, B., "The Rigidity of Graphs," *Transactions of the American Mathematical Society*, Vol. 245, Nov. 1978, pp. 279–289. doi:10.2307/1998867

[27] Sard, A., "The Measure of the Critical Values of Differentiable Maps,"*Bulletin of the American Mathematical Society*, Vol. 48, No. 12, 1942.

[28] Laman, G., "On Graphs and Rigidity of Plane Skeletal Structures," *Journal of Engineering Mathematics*, Vol. 4, No. 4, 1970, pp. 331–340. doi:10.1007/BF01534980